HHS Public Access

Author manuscript

J Oral Pathol Med. Author manuscript; available in PMC 2019 May 01.

Published in final edited form as:

J Oral Pathol Med. 2018 May ; 47(5): 484–491. doi:10.1111/jop.12705.

Visualizing the Effects of Metformin on Tumor Growth, Vascularity and Metabolism in Head and Neck Cancer

Aparajita Verma[1,2], **Laurie. J. Rich**[1], **Vincent Chong Vui King**[1], and **Mukund Seshadri**[1,2,3,*]

[1]Department of Dentistry and Oral Oncology, Roswell Park Cancer Institute, Buffalo, New York 14263

[2]Department of Molecular and Cellular Biophysics and Biochemistry, Roswell Park Cancer Institute, Buffalo, New York 14263

[3]Department of Head and Neck Surgery, Roswell Park Cancer Institute, Buffalo, New York 14263

Abstract

Background—The anti-diabetic drug Metformin (Met) is believed to inhibit tumor proliferation by altering the metabolism of cancer cells. In this study, we examined the effects of on tumor oxygenation, metabolism and growth in head and neck squamous cell carcinoma (HNSCC) using non-invasive multimodal imaging

Materials and Methods—Severe combined immunodeficient (SCID) mice bearing orthotopic FaDu HNSCC xenografts were treated with Met (200 mg/kg, i.p.) once daily for 5 days. Tumor oxygen saturation (%sO_2) and hemoglobin concentration (HbT) were measured using photoacoustic imaging (PAI). Fluorescence imaging was employed to measure intratumoral uptake of 2-deoxyglucosone (2-DG) following Met treatment while magnetic resonance imaging (MRI) was utilized to measure tumor volume. Correlative immunostaining of tumor sections for markers of proliferation (Ki67) and vascularity (CD31) was also performed.

Results—At 5 days post Met treatment, PAI revealed a significant increase ($p<0.05$) in %sO_2 and HbT levels in treated tumors compared to untreated controls. Fluorescence imaging at this time point revealed a 46% decrease in mean 2-DG uptake compared to controls. No changes in hemodynamic parameters were observed in mouse salivary gland tissue. A significant decrease in Ki-67 staining ($p<0.001$) and MR-based tumor volume was also observed in Met-treated tumors compared to controls with no change in CD31+ vessel count following Met therapy.

Conclusion—Our results provide, for the first time, direct in vivo evidence of Met-induced changes in tumor microenvironmental parameters in HNSCC xenografts. Our findings highlight the utility of multimodal functional imaging for non-invasive mapping of the effects of Met in HNSCC.

Correspondence: Dr. Mukund Seshadri, Roswell Park Cancer Institute, Elm and Carlton streets, Buffalo, New York 14263, Ph: 716-845-1552, Mukund.Seshadri@roswellpark.org.

CONFLICTS OF INTEREST

The authors do not have any conflicts of interest to disclose. The funding sponsors had no role in the design of the study, collection, analyses, or interpretation of data, writing of the manuscript, and in the decision to publish the results.

Keywords

head and neck squamous cell carcinoma; metformin; tumor hypoxia; photoacoustic imaging; fluorescence; MRI

INTRODUCTION

Head and neck cancers represent a major human health concern affecting over half a million individuals worldwide every year (1). In the United States, ~50,000 new cases are reported annually, a majority of whom present with locally advanced disease (2). The standard of care for head and neck squamous cell carcinomas (HNSCC) involves a combination of surgery, chemotherapy and radiation therapy (RT) (3). However, response rates of HNSCC patients to current treatment regimens are relatively modest. Furthermore, HNSCC patients suffer from poor quality of life due to long-term radiation toxicities (4). While development of image-guided radiation delivery schemes has minimized collateral radiation damage to normal tissues in the head and neck region, tumor hypoxia is a major therapeutic hurdle that significantly diminishes radiotherapeutic efficacy (5, 6). As a result, there has been increased interest in developing approaches that can alleviate tumor hypoxia to improve RT (7). These studies have focused on vascular remodeling using anti-angiogenic agents such as Bevacizumab to 'normalize' blood vessels (8), hypoxia targeting bio-reductive drugs (9) or methods such as hyperbaric oxygen therapy to increase oxygen delivery (10).

An alternative strategy to alleviate tumor hypoxia is to modulate the metabolism and decrease oxygen consumption of tumor cells (11). In this regard, the Food and Drug Administration (FDA) approved anti-diabetic drug, Metformin (Met), has been shown to target cellular respiration by inhibiting mitochondrial complex I in the electron transport chain and inhibit glycometabolism of HNSCC cells *in vitro* (12). Metformin has been previously been shown to exhibit chemopreventive activity alone and in combination with agents such as Curcumin against HNSCC (13, 14). The effect of Met on proliferation and tumor growth has also been recently studied in xenograft models of HNSCC (15). These published studies have mostly utilized histologic and immunohistochemical markers (e.g. EF5) to evaluate the effects of Met *in vivo*. Although useful, these techniques are invasive in nature and provide a limited ex-vivo assessment of Met –induced changes in tumors. In contrast, non-invasive imaging methods can provide direct evidence of changes in tumor growth, metabolism and oxygenation *in situ*.

The overall goal of the present study was to utilize a non-invasive, multi-modal imaging approach to examine the impact of Met in an orthotopic xenograft model of HNSCC. To date, the effect of Met on tumor oxygenation in HNSCC has not been reported. To address this gap in knowledge, we employed photoacoustic imaging (PAI), a non-invasive hybrid imaging method that enables visualization and quantification of tumor oxygen saturation ($\%sO_2$) by exploiting differences in optical absorption characteristics of oxygenated and de-oxygenated hemoglobin (16, 17). Experimental studies were conducted in an orthotopic model of HNSCC to determine if PAI could provide non-invasive assessment of improved tumor oxygenation following Met therapy. In addition to PAI, the *in vivo* effects of Met on

tumor growth, and metabolism were studied using magnetic resonance imaging (MRI) and fluorescence imaging (FI), respectively. Immunohistochemical staining of tumors for markers of proliferation (Ki67) and vascularity (CD31) were used to validate the effects of Met within the tumor microenvironment.

MATERIALS AND METHODS

Animals

Eight-to-twelve week old female CB.17 (C.B-Igh-1^b/IcrTac-$Prkdc^{scid}$; weighing ~20 g) severe combined immunodeficient (SCID) mice bred in-house at Roswell Park Cancer Institute (RPCI) were used. Animals were housed in sterile micro isolator cages on 12-h light/dark cycles in a HEPA-filtered pathogen-free environment and provided with standard chow/water. FaDu human HNSCC cells were cultured in complete Dulbecco's modified eagle medium containing 10% fetal bovine serum and 1% penicillin-streptomycin and incubated at 5% CO_2. Orthotopic FaDu tumors were established according to previously described procedures (18). Adequate measures were taken to minimize pain or discomfort in accordance with NIH guidelines regarding the care and use of animals in research. All experimental procedures were performed in accordance with approved protocols at RPCI.

Metformin treatment

Metformin (Sigma-Aldrich, USA) powder was dissolved in sterile distilled water and administered at a dose of 200 mg/kg by intraperitoneal (i.p.) injection (5 days). Control animals received i.p. injections of water. Animals were monitored daily for changes in body weight and observed for clinical signs of morbidity (ruffled fur, inability to consume food/water and labored breathing) and euthanized as per institutional guidelines.

Photoacoustic imaging with co-registered ultrasound

PAI and B-mode ultrasound (US) images were acquired using a commercially available 21 MHz linear array transducer system (Vevo LAZR; VisualSonics Inc., Toronto) as described previously (19). Prior to imaging, animals were anesthetized, secured to the imaging platform, and hair removed to permit light delivery. Quantification of $\%sO_2$ and total hemoglobin concentration (HbT) was performed by manually tracing the region of interest (ROI) around the tumor excluding the skin throughout a 3D stack using Vevo LAB (Ver 1.7.2). For salivary gland measurements, an ROI was traced around the single, central slice of salivary gland excluding the skin to calculate the $\%sO_2$ and HbT (19). Color maps representing $\%sO_2$ were displayed using a color look-up table superimposed on spatially co-registered B-mode US images.

Fluorescence imaging

Intratumoral uptake of the fluorescent probe, 2-DeoxyGlucosone (2-DG; Peak excitation: 750 nm, Peak Emission: 820 nm; Perkin Elmer, USA) (20) was visualized and quantified using the Xenogen IVIS imaging system (Caliper Life Sciences, Alameda, CA, USA). Fluorescence imaging was performed 3 hours after injection of 100 μl of 2-DG (10 nM, i.v.). Images were processed using Living Image Software (Caliper Life Sciences, Alameda, CA, USA) by tracing out of a region of interest (ROI) covering the tumor and reported as

normalized signal intensity (Normalized signal intensity = Mean signal intensity of ROI/ROI area).

Magnetic resonance imaging

MRI examinations were performed in a 4.7 T/33-cm horizontal bore magnet (GE NMR Instruments, Fremont, CA) incorporating AVANCE digital electronics (Bruker Biospec. Bruker Medical Inc.,Billerica, MA, USA). Mice were anesthetized using 2.5% Isoflurane and secured in a form-fitted, MR compatible mouse sled (DAZAI Research Instruments, Toronto, Canada) equipped with temperature and respiratory monitoring sensors. Multi-slice, T2-weighted spin echo images were acquired on the axial plane for each mouse to measure tumor volume using the following parameters; matrix size: 256 × 192, TE/TR= 41/2500 ms, slice thickness: 1mm, field of view (FOV): 3.2 × 3.2 cm, number of slices = 20. An ROI was manually traced around the entire tumor on multiple slices to calculate tumor volume as described previously (18).

Immunohistochemistry

Tumors from control and Met-treated animals were excised and placed in fixative for immunostaining and histology. Tumor proliferation index was estimated using Ki-67 stained specimens (mAb; Dako - M7240). Five random areas were captured at 40 × magnification and analyzed using NIH Image J software (NIH, Maryland). Staining intensity was categorized into 1 = negative/no stain, 2 = weak, 3 = moderate and 4 = strong. For each image, 100 cells with nuclei were assessed for staining intensity and assigned a value from 1 to 4. The scores were assessed by an observer who was blinded to the identity of the samples. The H-scores for Ki-67 was calculated as the sum scores of all the 500 cells per sample. Microvessel density was estimated by counting CD31 (MEC13; BD Pharmingen – 550274) positive endothelial clusters with a visible lumen on stained tissue sections. Stained slides were scanned and digitized using Scanscope XT (Aperio Technologies, Vista, CA).

Study design and statistical considerations

The experimental outline of the study to employ multimodal imaging (MRI, US and FI) for examining the response of orthotopic HNSCC xenografts to Metformin (Met) treatment is shown in Fig. 1A. Female SCID mice bearing orthotopic FaDu tumors (n = 10) were treated with Met at a dose of 200 mg/kg by intraperitoneal (i,p.) injection for five days. Control animals (n = 7) received water for the same duration. MRI was performed to measure tumor volume before and after treatment. PAI and FI were used to measure tumor hemodynamics and 2-DG uptake 24h after completion of treatment. Tumors were excised from control (n=5) and treated (n=7) animals to perform immunohistochemical analysis following completion of imaging. All statistical analysis was performed using GraphPad Prism (GraphPad Software, San Diego, CA). Reported values represent mean ± standard error. Difference in imaging parameters between control and treated tumors were analyzed using unpaired t-test. Two-tailed unpaired t-test was performed to analyze the difference in oxygen saturation between control and treated groups. P-values <0.05 were considered statistically significant.

RESULTS

Antitumor activity of Met against orthotopic HNSCC xenografts

We utilized non-invasive MRI to examine the antitumor activity of Met on the growth of orthotopic FaDu HNSCC xenografts. MRI of tumor-bearing mice was performed at baseline (3 days prior to start of treatment) and on Day 5 after five doses of Met (200 mg/kg, i.p.) to measure tumor response to therapy. The panel of images shown in Fig. 1B represents non-contrast enhanced T2-weighted (T2W) images of control and Met-treated animals bearing orthotopic FaDu tumors (*outlined in yellow*). Tumor volumes in both groups were comparable prior to start of Met treatment (Fig. S1A). MRI provided visual evidence of tumor growth inhibition with Met treatment compared to controls. Quantitative estimates of tumor volume calculated from multi-slice T2W images confirmed a significant reduction ($p<0.05$) in tumor growth following Met therapy compared to untreated controls (Fig. 1C).

PAI of changes in tumor oxygen saturation and hemoglobin concentration following Met treatment

We evaluated the change in tumor sO_2 and HbT following Met treatment using US/PAI. B-mode US (Fig. 2A, top row) enabled visualization of orthotopic FaDu tumor growth (*outlined in white*) in mice. Co-registered parametric maps of oxygen saturation (Oxy-sat; Fig. 2A, 2nd row) and hemoglobin concentration (HbT; Fig. 2A, third row) enabled mapping of tumor hemodynamics in control and Met treated tumors. Pseudo-colorized maps showed a visible increase in oxygen saturation on day 5 post Met treatment compared to control tumors (two tumors per type are shown). Quantitative analysis revealed a significant increase ($p<0.05$) in $\%sO_2$ (Fig. 2B) following Met treatment (62.3 ± 3.9) compared to untreated controls (49.9 ± 3.2). Difference in HbT was also significant ($p<0.05$) between the two groups (Fig. 2C).

Fluorescence imaging of intratumoral 2-DG uptake following Met treatment

Next, we evaluated the impact of Met treatment on tumor metabolism using fluorescence imaging. The fluorescent probe 2-DG was administered to tumor-bearing mice in both experimental groups. Fig. 2A (bottom row) shows fluorescence images of two control and Met-treated animals bearing orthotopic FaDu tumors post injection of 2-DG. A visible decrease in fluorescence intensity in Met treated tumors compared to the controls. Normalized fluorescence signal intensity measurements revealed a 46% decrease in mean 2-DG uptake in treated tumors as compared to controls. However, this change was not statistically significant (Fig. 2D).

Effect of Met treatment on salivary gland hemodynamics

To measure the effect of Met on normal tissue hemodynamics, we assessed change in $\%sO_2$ and HbT (Fig. 3) of mouse salivary glands. Fig. 3A shows B-mode US image (top), pseudocolorized PA-based maps of oxygen saturation (Oxy-sat) and hemoglobin concentration (HbT) of the mouse salivary gland (outlined in white). As illustrated visually (Fig. 3A) Met treatment did not result in any change in salivary gland hemodynamics of

mice. Quantitative estimates of $\%sO_2$ (Fig. 3B) and HbT levels in the salivary glands (Fig. 3C) after five days of treatment with metformin were comparable to controls.

Immunohistochemical assessment of HNSCC vascular and cellular response to Met

To validate our imaging results, tumors from both the groups (controls n=5, treated n=7) were excised from the animals following completion of treatment and imaged for immunostaining and histopathological assessment. The tumors were stained for the proliferation marker, Ki-67, and the vascular marker, CD-31 (Fig. 4). Fig. 4A shows photomicrographs of control and Met-treated tumors stained for CD31 (top) and Ki-67 (bottom). CD31 immunostaining did not reveal significant difference in vessel counts between control and treated tumors (Fig. 4B). Consistent with MRI results, a significant decrease in staining for Ki-67 was seen in metformin-treated mice (66.29 ± 2.765) compared to control mice (100 ± 3.352) (Fig. 4C).

DISCUSSION

There has been considerable preclinical and clinical investigation into the chemopreventive and therapeutic potential of Met against HNSCC (11–15; 21). As such, Met is undergoing clinical evaluation in ‘window of opportunity’ trials in HNSCC patients (22, 23). A recent clinical study has demonstrated that Met is also well tolerated in HNSCC patients (23). In the present study, we examined the effects of Met treatment within the tumor microenvironment using multimodal imaging. Table 1 summarizes the key observations of our study. The dose and schedule of Met used in our study was selected based on preliminary dose response studies conducted in our laboratory using subcutaneous FaDu xenografts (Fig. S1B). This dose of Met was well tolerated without any evidence of toxicity based on body weight measurements.

We utilized non-invasive MRI to measure tumor volume changes following Met treatment as it offers superior soft tissue contrast without the use of ionizing radiation or radioactive isotopes. MRI enabled visualization and accurate quantification of tumor burden in the oral cavity of mice. As a single agent, we observed a modest but significant inhibition of tumor growth (MRI). Consistent with our MRI results and published observations in preclinical models (13–15), immunostaining of tumor section for the proliferation marker, Ki67 showed a reduction in Met-treated tumors compared to controls.

Fluorescence imaging was used to examine the intratumoral uptake of optically labeled 2-DG probe following Met treatment. Higher uptake of the fluorescent 2-DG probe has been reported in hypoxic regions of Cal33 HNSCC xenografts, presumably due to the Warburg effect (20). In our study, Met- treated tumors showed lower 2-DG uptake compared to control tumors. However, the difference between the two groups was not significant. Unlike MRI or PAI measurements, in the present study, fluorescence imaging measurements were performed in 2D and can therefore be influenced by the depth of tumors. In addition, Tseng et al. have shown that uptake of NIR 2-DG probes is influenced by the enhanced permeability and retention (EPR) effect and tumor volume (24). It is therefore plausible that the effect of Met on tumor volume and permeability could have also contributed to the fluorescence signal intensity measurements.

Non-invasive PAI revealed an increase in tumor $\%sO_2$ following Met therapy. To the best of our knowledge, this is the first study to demonstrate modulation of tumor oxygenation with Met treatment in HNSCC using PAI based on endogenous contrast. In HNSCC patients undergoing RT, salivary glands are often in the radiation field. As a result, the glands experience collateral radiation damage that results in long-term symptoms such as dry mouth and recurrent oral infections (25). In this regard, bio-distribution studies in mice and humans have shown accumulation of Met in salivary glands (26, 27). We therefore examined the changes in $\%sO_2$ of salivary glands following Met treatment using PAI. No significant change in $\%sO_2$ and HbT of salivary glands was observed following Met administration. This suggests that Met selectively improves tumor oxygenation without altering normal tissue hemodynamics, further supporting its potential utility as a radiosensitizer.

To validate our PAI data, we performed immunostaining of tumor sections for the endothelial marker, CD31. While PAI of tumors showed an increase in $\%sO_2$ and HbT, CD31 immunostaining did not reveal any change in vessel count between control and treated tumors. This observation is supportive of Met induced reduction in oxygen consumption and is consistent with a previous report by Zannella *et al.*, (28) in which Met resulted in decreased hypoxia. In the study by Zannella and co-workers, the ability of Met to modify tumor hypoxia was studied in experimental models of prostate and colorectal cancer using positron emission tomography (PET) and immunostaining of tumors for pimonidazole (28). However, PET is expensive and requires administration of radioactive tracers. Furthermore, it has been shown that activation of AMPK following Met treatment may confound results from 18F-FDG PET (29). In comparison, PAI can provide quantitative readouts of oxygen saturation and hemoglobin concentration in a rapid and cost-effective manner without the use of radioactive isotopes. Consistent with our PAI observations, a recent study by Wang et al. has shown that Metformin suppresses hypoxia-induced excessive angiogenesis in peri-necrotic regions of tumors by elevating tumor perfusion (30).

In conclusion, using multimodal imaging we have demonstrated the effects of Met on tumor oxygenation, metabolism and proliferation in HNSCC. However, we recognize the limitations in our study. The observations in our study are limited to only one xenograft model and consisted of short-term response assessment. Future studies should address the limitations of our study by investigating the effects and mechanisms of Met-mediated effects on tumor oxygenation in multiple HNSCC models established in diabetic and non-diabetic mice. Given the widespread interest in using Met to enhance radiotherapeutic efficacy, further examination of Met in combination with chemotherapy and radiation is also warranted. In this regard, our observations in the subcutaneous tumor model (Fig. S1B) revealed a significant increase in tumor oxygen saturation on d5 which returned to baseline levels (48 hours post cessation of Met therapy) suggestive of the transient nature of metformin changes in oxygenation *in vivo*. It would therefore be critical to define an optimal schedule and sequence of administering Met in combination with radiotherapy to maximize therapeutic benefit. In this regard, our results highlight the potential of PAI as a powerful, non-invasive tool for real-time assessment of early changes in tumor oxygenation following Met therapy that could potential enable identification of an optimal window for administering RT in combination with Met.

Supplementary Material

Refer to Web version on PubMed Central for supplementary material.

Acknowledgments

This work was supported by grants from the NIH/NCI R01CA204636, NIH/OD S10OD010393 and the Alliance Foundation of Western New York (all to M.S), and utilized shared resources supported the NCI Cancer Center Support Grant P30CA016056 (Johnson, CS).

References

1. Hussein AA, Helder MN, de Visscher JG, et al. Global incidence of oral and oropharynx cancer in patients younger than 45 years versus older patients: a systematic review. Eur J Cancer. 2017; 82:115–27. [PubMed: 28654785]
2. Siegel RL, Miller KD, Jemal A. Cancer statistics, 2017. CA Cancer J Clin. 2017; 67:7–30. [PubMed: 28055103]
3. Adelstein D, Gillison ML, Pfister DG, et al. NCCN Guidelines Insights: Head and Neck Cancers. J Natl Compr Canc Netw. 2017; 15:761–70. [PubMed: 28596256]
4. Høxbroe Michaelsen S, Grønhøj C, Høxbroe Michaelsen J, Friborg J, von Buchwald C. Quality of life in survivors of oropharyngeal cancer: a systematic review and meta-analysis of 1366 patients. Eur J Cancer. 2017; 78:91–102. [PubMed: 28431302]
5. Harris AL. Hypoxia—a key regulatory factor in tumour growth. Nat Rev Cancer. 2002; 2:38–47. [PubMed: 11902584]
6. Dewhirst MW, Cao Y, Moeller B. Cycling hypoxia and free radicals regulate angiogenesis and radiotherapy response. Nat Rev Cancer. 2008; 8:425–37. [PubMed: 18500244]
7. Curtis KK, Wong WW, Ross HJ. Past approaches and future directions for targeting tumor hypoxia in squamous cell carcinomas of the head and neck. Crit Rev Oncol Hematol. 2016; 103:86–98. [PubMed: 27247118]
8. Jain RK. Normalizing tumor vasculature with anti-angiogenic therapy: a new paradigm for combination therapy. Nat Med. 2001; 7:987–9. [PubMed: 11533692]
9. Overgaard J, Hansen HS, Overgaard M. A randomized double-blind phase III study of nimorazole as a hypoxic radiosensitizer of primary radiotherapy in supraglottic larynx and pharynx carcinoma. Results of the Danish Head and Neck Cancer Study (DAHANCA) Protocol 5-85. Radiother Oncol. 1998; 46:135–46. [PubMed: 9510041]
10. Overgaard J, Horsman MR. Modification of hypoxia-induced radioresistance in tumors by the use of oxygen and sensitizers. Sem Radiat Oncol. 1996; 6:10–21.
11. Sandulache VC, Skinner HD, Ow TJ, et al. Individualizing antimetabolic treatment strategies for head and neck squamous cell carcinoma based on TP53 mutational status. Cancer. 2012; 118:711–21. [PubMed: 21720999]
12. Rêgo DF, Elias ST, Amato AA, De Luca Canto G, Guerra ENS. Anti-tumor effects of metformin on head and neck carcinoma cell lines: A systematic review. Oncol Lett. 2017; 13:554–66. [PubMed: 28356929]
13. Vitale-Cross L, Molinolo AA, Martin D, et al. Metformin prevents the development of oral squamous cell carcinomas from carcinogen-induced premalignant lesions. Cancer Prev Res. 2012; 5:562–73.
14. Siddappa G, Kulsum S, Ravindra DR, et al. Curcumin and metformin-mediated chemoprevention of oral cancer is associated with inhibition of cancer stem cells. Mol Carcinog. 2017; 56:2446–60. [PubMed: 28618017]
15. Tassone P, Domingo-Vidal M, Whitaker-Menezes D, et al. Metformin effects on metabolic coupling and tumor growth in oral cavity squamous cell carcinoma coinjection xenografts. Otolaryngol Head Neck Surg. 2017; [Epub ahead of print]. doi: 10.1177/0194599817746934

16. Laufer J, Elwell C, Delpy D, Beard P. In vitro measurements of absolute blood oxygen saturation using pulsed near-infrared photoacoustic spectroscopy. Phys Med Biol. 2005; 50:4409–28. [PubMed: 16148401]
17. Hu S, Wang LV. Photoacoustic imaging and characterization of the microvasculature. J Biomed Opt. 2010; 15:011101. [PubMed: 20210427]
18. Seshadri M, Toth K. Acute vascular disruption by 5,6-dimethylxanthenone-4-acetic Acid in an orthotopic model of human head and neck cancer. Transl Oncol. 2009; 2:121–7. [PubMed: 19701496]
19. Rich LJ, Seshadri M. Photoacoustic monitoring of tumor and normal tissue response to radiation. Sci Rep. 2016; 6:21237. [PubMed: 26883660]
20. Nakajima EC, Laymon C, Oborski M, et al. Quantifying metabolic heterogeneity in head and neck tumors in real time: 2-DG uptake is highest in hypoxic tumor regions. PLoS One. 2014; 9:e102452. [PubMed: 25127378]
21. Lerner MZ, Mor N, Paek H, Blitzer A, Strome M. Metformin prevents the progression of dysplastic mucosa of the head and neck to carcinoma in nondiabetic patients. Ann Otol Rhinol Laryngol. 2017; 126:340–3. [PubMed: 28103701]
22. Chang PH, Yeh KY, Wang CH, et al. Impact of metformin on patients with advanced head and neck cancer undergoing concurrent chemoradiotherapy. Head Neck. 2017; 39:1573–7. [PubMed: 28449193]
23. Curry J, Johnson J, Tassone P, et al. Metformin effects on head and neck squamous carcinoma microenvironment: Window of opportunity trial. Laryngoscope. 2017; 127:1808–15. [PubMed: 28185288]
24. Tseng JC, Wang Y, Banerjee P, Kung AL. Incongruity of imaging using fluorescent 2-DG conjugates compared to 18F-FDG in preclinical cancer models. Mol Imaging Biology. 2012; 14:553–60.
25. Strojan P, Hutcheson KA, Eisbruch A, et al. Treatment of late sequelae after radiotherapy for head and neck cancer. Cancer Treat Rev. 2017; 59:79–92. [PubMed: 28759822]
26. Wilcock C, Bailey CJ. Accumulation of metformin by tissues of the normal and diabetic mouse. Xenobiotica. 1994; 24:49–57. [PubMed: 8165821]
27. Gormsen LC, Sundelin EI, Jensen JB, et al. In vivo imaging of human 11C-Metformin in peripheral organs: dosimetry, biodistribution, and kinetic analyses. J Nucl Med. 2016; 57:1920–6. [PubMed: 27469359]
28. Zannella VE, Dal Pra A, Muaddi H, et al. Reprogramming metabolism with metformin improves tumor oxygenation and radiotherapy response. Clin Cancer Res. 2013; 19:6741–50. [PubMed: 24141625]
29. Habibollahi P, van den Berg NS, Kuruppu D, Loda M, Mahmood U. Metformin—an adjunct antineoplastic therapy—divergently modulates tumor metabolism and proliferation, interfering with early response prediction by 18F-FDG PET imaging. J Nuc Med. 2013; 54:252–8.
30. Wang JC, Li GY, Li PP, et al. Suppression of hypoxia-induced excessive angiogenesis by metformin via elevating tumor blood perfusion. Oncotarget. 2017; 8:73892–904. [PubMed: 29088755]

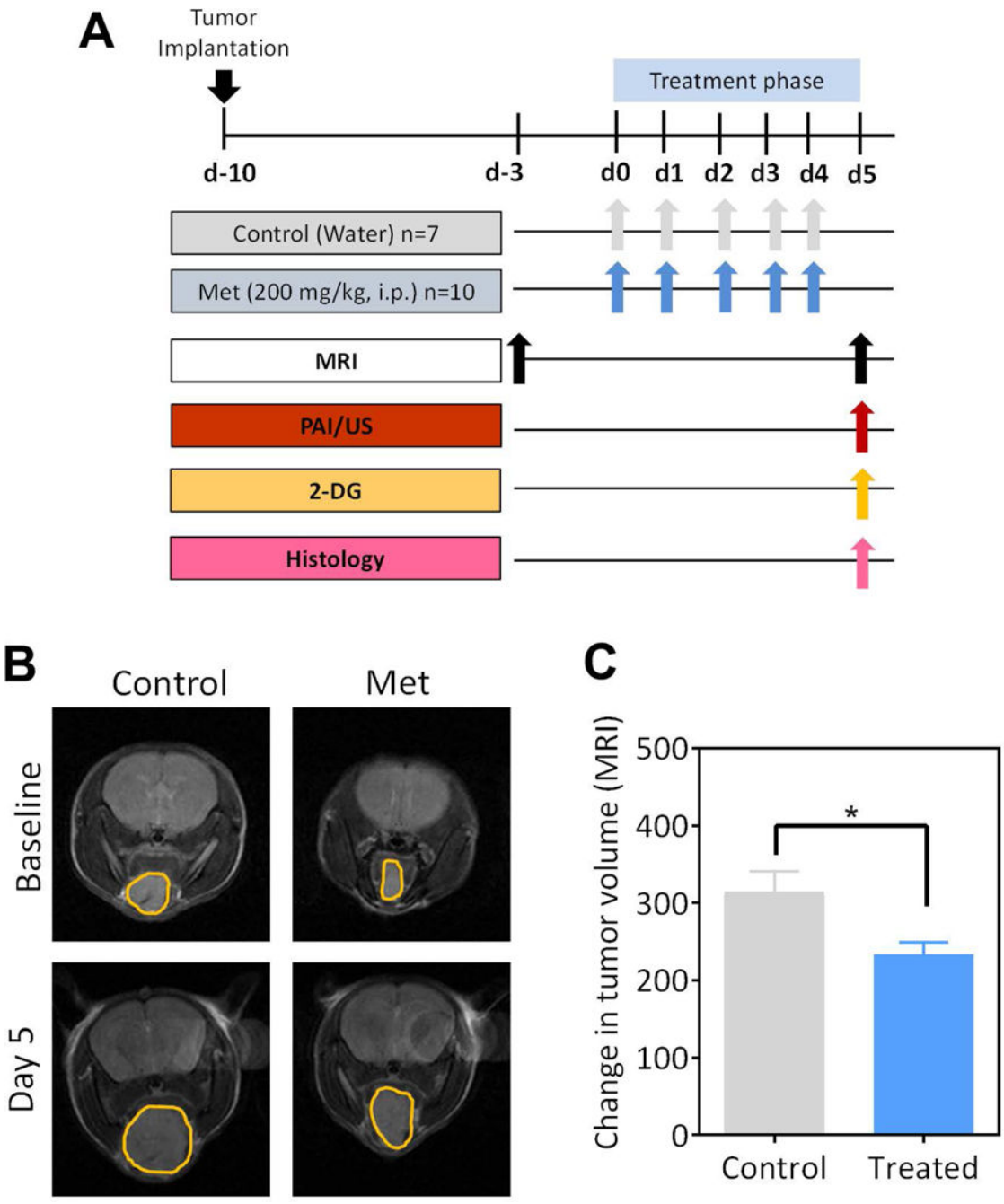

Figure 1.

(A) Schematic shows the experimental outline for multimodal imaging-based assessment HNSCC response to Metformin (Met) treatment. MRI was performed to measure tumor volume before and after treatment. PAI and FI were used to measure tumor hemodynamics and 2-DG uptake, respectively at the end of treatment. Tumors were excised for immunohistochemical analysis following completion of imaging. (**B**) Axial non-contrast enhanced T2-weighted (T2W) images of control and Met-treated animals bearing orthotopic FaDu tumors at baseline (pretreatment) and on day 5 post treatment. The tumor has been

outlined in yellow on all the images. (**C**) Bar graph shows change in MR-based tumor volumes from baseline to day 5 post treatment in control and Met treated animals.

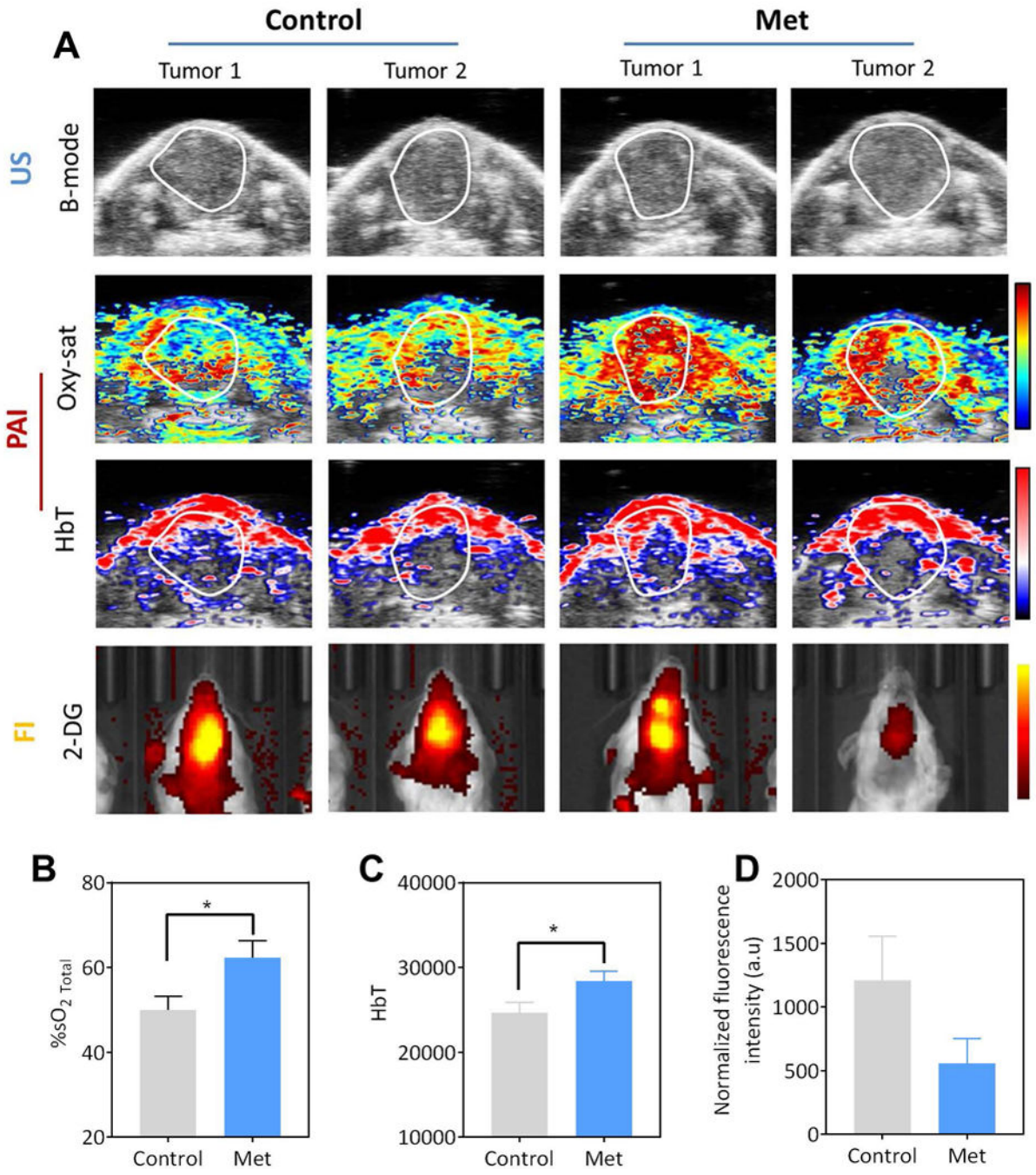

Figure 2. Photoacoustic and fluorescence imaging of tumor response to Metformin therapy

(**A**) B-mode US (top row) images of control and Met treated orthotopic FaDu tumors (*outlined in white*). Images for two different tumors are shown. Parametric maps of tumor $\%sO_2$ (oxy-sat; 2nd row) and hemoglobin concentration (HbT; 3rd row) calculated using PAI are also shown. Corresponding fluorescence images (FI; 2-DG; bottom row) showed a visible decrease in fluorescence intensity in Met treated tumors compared to the controls. Quantitative measurements of tumor oxygen saturation ($\%sO_2$; **B**), HbT (**C**) and normalized fluorescence signal intensity (**D**) of control and metformin treated tumors. *p<0.05

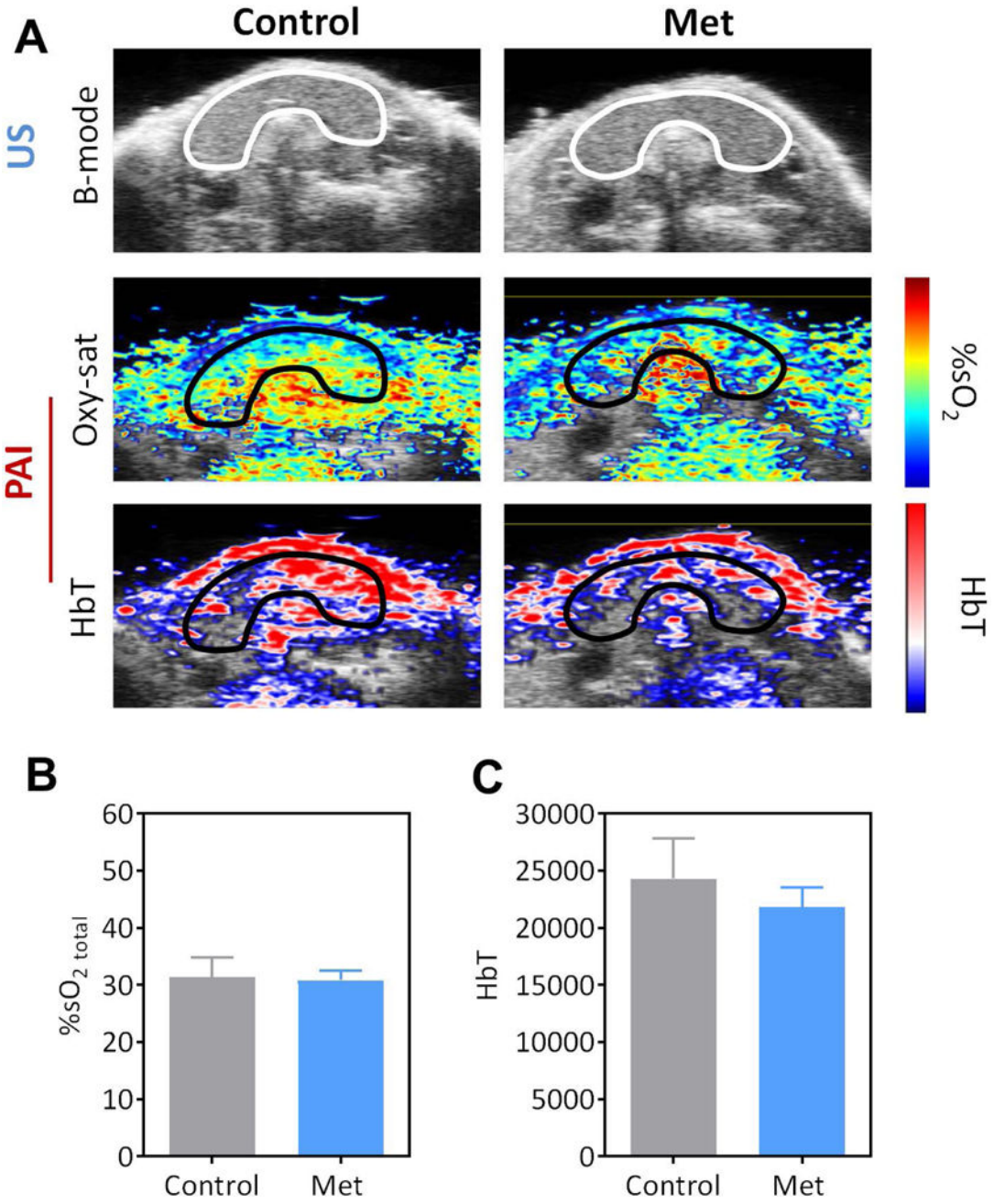

Figure 3. Effect of Metformin treatment on salivary gland hemodynamics

(**A**) Panel of images represent B-mode US (*top row; outlined in white)*, $\%sO_2$ (Oxy-sat; *middle row*) and hemoglobin concentration (HbT; *bottom row*) maps of salivary glands in control and Met treated animals. Pseudo-colorized maps of Oxy-sat and HbT of salivary glands (*outlined in black)* were superimposed on B-mode US images. Bar graphs showing quantified values of salivary gland oxygen saturation ($\%sO_2$ total; **B**) and HbT (**C**) are also shown. n=3 per group.

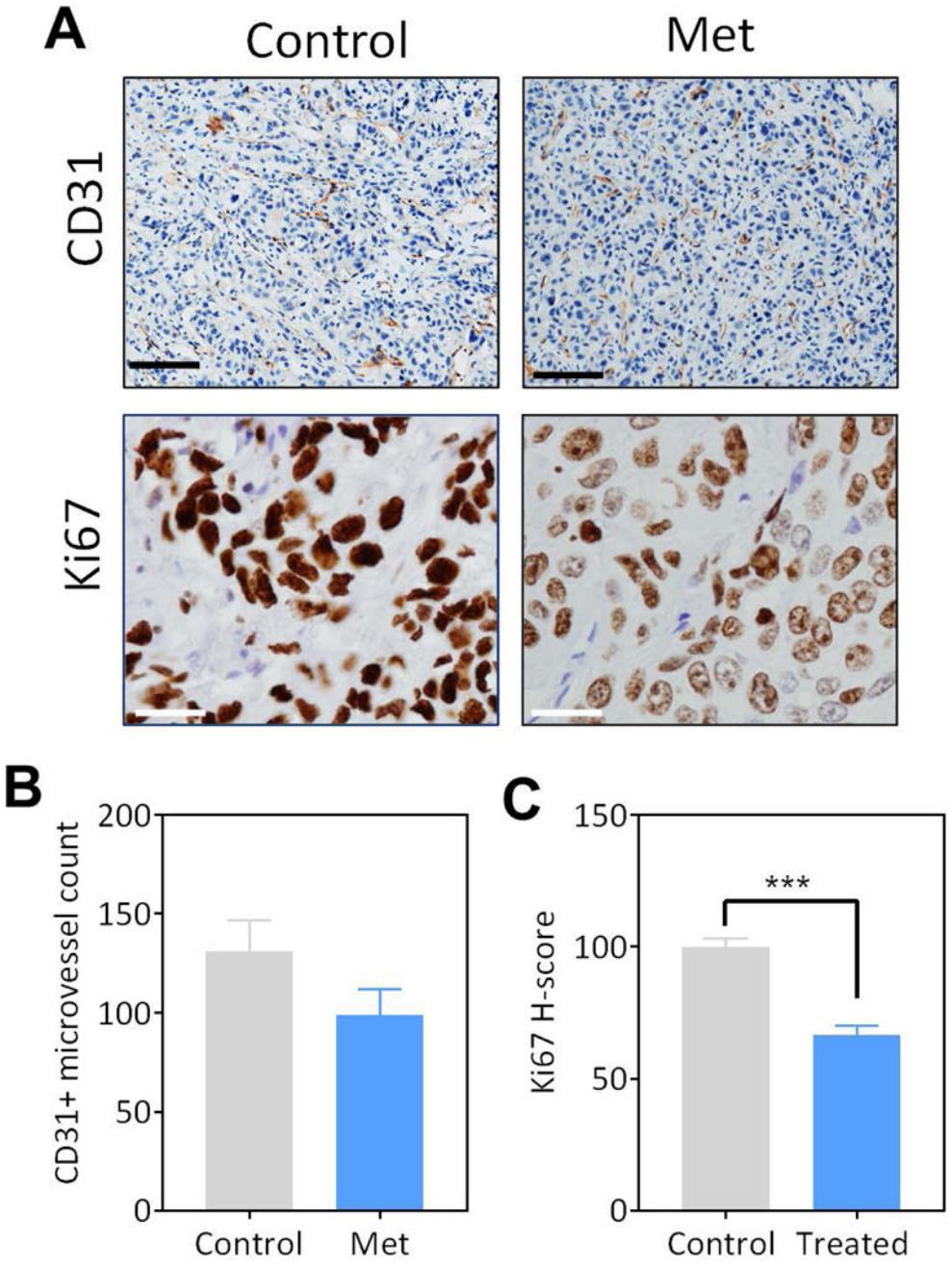

Figure 4. Immunohistochemical assessment of tumor growth, vascularity and proliferation in response to Metformin treatment in orthotopic FaDu xenografts

(**A**) Photomicrographs of CD31 (20 × magnification; scale bar represents 100μm) and Ki67 (40 × magnification; scale bar represents 50μm) immunostained tumor sections of orthotopic FaDu tumors obtained from control and Metformin treated animals. Quantitative measurements of CD31+ microvessel counts (**B**) and H-score for Ki-67 (**C**) are shown.*p<0.05, ***p<0.001

Table 1
Response of orthotopic FaDu xenografts to Metformin

Table summarizes the imaging and immunohistochemical measurements obtained from all the experimental studies. Values are reported as mean ± standard error.

Method	Measured Parameter	Control	Metformin	Observation
MRI	Tumor volume (mm^3)	315.1 ± 26	233.7 ± 16 *	Significant decrease at d5
PAI	Oxygen saturation (%sO_2)	49.9 ± 3.2	62.3 ± 3.9 *	Significant increase at d5
	HbT (a.u.)	24670 ± 1199	28444 ± 1148 *	Significant increase at d5
Fluorescence imaging (2-DG)	Normalized fluorescence intensity (a.u.)	1211 ± 348	559 ± 192	No significant change
CD31-immunostaining	Microvessel count	131 ± 15	99 ± 13	No significant change
Ki67 immunostaining	H-score	100 ± 2.9	66 ± 3.5 ***	Significant reduction

* $p<0.05$

*** <0.001 between control and treatment groups.